Multi-Satellite Interferometric SAR System

Andon Lazarov[1,2], Chavdar Minchev[3] and Dimitar Minchev[1]
[1] *Burgas Free University, 62 SanStefano Str., Burgas, Bulgaria*
[2] *K.N. Toosi University of Technology, Tehran, Iran*
[3] *Shumen University, 115 Universitetska Str. Shumen, Bulgaria*
lazarovr@bfu.bg, chavdar_minchev@yahoo.com, mitko@bdu.bg

Keywords: InSAR, Multi-satellite system, InSAR geometry, InSAR signal model.

Abstract: In the present work a multi-satellite SAR system is considered. Between every pair of SAR satellites an interferometric concept is implemented. It allows the height of each pixel on the surface to be evaluated with high precision and a three dimensional map to be created. InSAR geometry is analytically described. Mathematical expressions for determination of current distances between SAR's and detached pixels on the ground, and principal InSAR parameters are derived. A model of linear frequency modulated (LFM) SAR signal with InSAR applications, reflected from the surface is developed. Correlation and spectral SAR image reconstruction algorithms and co-registration procedure are described. To verify the correctness of the signal model and image reconstruction and co-registration algorithm numerical experiment is carried out.

1 INTRODUCTION

Synthetic Aperture Radar (SAR) is a coherent active microwave imaging instrument. Back scattered information of a target is recorded as a complex signal with amplitude and phase information. Interferometric SAR (InSAR) technique makes use of phase difference information extracted from two complex valued SAR images acquired from different orbit positions. This information is useful in measuring several geophysical quantities such as topography, slope, deformation (volcanoes, earthquakes, ice fields), glacier studies, vegetation growth etc (Rott, H., et al., 2003, Rott, H., et al. 1999, Massonet, D., et al. 1998, Henry, E. et al. 2004, Rott, H. et al. 2000, Berardino, P., et al. 2002, Berardino, P., et al. 2003).

SAR interferometry was first used for topographic mapping by Graham (Graham, L.C, 1974). The first practical results were obtained by Zebker and Goldstein (Zebker, H.A., Goldstein, R.M., 1986) using side looking airborne radar. Studies on interferometric SAR were extended after the launch of ERS-1 and ERS-2, and Envisat satellites (Feigl, K.L., et al. 2002). The number of scientific research on InSAR technology has also exploded since the launch of new satellites such as of class Sentinel.

In order to obtain SAR interferometric data, two spatially separated antennas, the physical separation of which is called the interferometric baseline, are mounted on a single platform or one antenna is mounted on a satellite and data sets are acquired by passing the same area twice. In the latter case, the interferometric baseline is formed by relating radar signals on repeat passes over the target area. This approach is called repeat-pass interferometry. SAR interferometry is a promising tool for mapping topography, detecting small surface displacement caused by earthquake, volcanic activity, and landslides and ice movement (Weston, J., et al. 2012, Feng, G. et al, 2010). There are various publications on estimating earthquake parameters using InSAR measurements (Gens, R., Van Genderen, J.L.,1996, Reilinger, R.E., 2000, Wright, T.J., et al. 2003, Liu-Zeng, J., et al. 2009, Sudhaus, H., et al. 2009).

Lazarov A., Minchev C. and Minchev D.
Multi-Satellite Interferometric SAR System.
DOI: 10.5220/0006226900330042
In *Proceedings of the Fifth International Conference on Telecommunications and Remote Sensing (ICTRS 2016)*, pages 33-42
ISBN: 978-989-758-200-4

The current emphasis in the satellite industry is on replacing large satellite platforms with one or more smaller satellites, i.e. there is increasing interest in the potential capabilities and applications of so-called mini satellites. A multi-satellite system is a group of mini satellites that fly within very close range of each other (e.g., 250 m - 5 km). These satellites coordinate their activities, so that they can use sparse array interferometry and synthetic aperture techniques to simulate a single, very large satellite. The multi-satellite system operates as a "virtual" satellite with a very large effective aperture, without the need for the heavy infrastructure that would be required to have a monolithic satellite with the equivalent aperture. The multi-satellite system approach has many advantages over a single large satellite: each spacecraft is smaller, lighter, simpler, and simpler to manufacture; economies of scale enable a multi-satellite system of many satellites to be less expensive to manufacture than a single satellite; multi-satellite system can adapt to the failure of any individual satellites, and failed satellites can be incrementally replaced; multi-satellite system can reconfigure the orbits of the satellites in the multi-satellite system to optimize for different missions.

In the present work a multi-satellite SAR system is considered. The multi-satellite system consists of mini satellites performing different roles. On one of them a SAR transmitter and receiver are activated, on the other only SAR receivers. Between every pair of SAR satellites an interferometric concept is implemented. It allows the height of each pixel on the surface to be evaluated with high precision and a three dimensional map to be created. The main goal of the work is to describe InSAR geometry with multiple satellites and derive mathematical expressions for definition of current distances between SAR's and detached pixels, and principal InSAR parameters and, as a result, a model of linear frequency modulated SAR signal with InSAR applications, reflected from the surface to be developed. In order to extract complex SAR images and intergerograms, correlation and spectral SAR image reconstruction algorithms is suggested and implemented.

The rest of the paper is organized as follow. In section II a 3-D InSAR geometry is analytically described. In section III SAR LFM transmitted waveform and model of deterministic SAR signal return are defined. In section IV SAR image reconstruction, co-registration, SAR interferogram generation, and iterative procedure for pixel height determination are analytically described. In section V results of numerical experiment are presented. In section VI conclusions are made.

2 InSAR GEOMETRY

2.1 Geometry and Kinematics' Equations

Assume a multi-satellite SAR system viewing three dimensional (3-D) surface presented by discrete resolution elements, pixels. Each of these pixels is defined by the third coordinate $z_{ij}(x_{ij}, y_{ij})$ in 3-D coordinate system $Oxyz$. The surface is illuminated by linear frequency modulated waveforms emitted by a transmitter mounted on one satellite. A_1, A_2 … A_n represent SAR receive antennas mounted on satellites viewing the same surface simultaneously. Between every pair $A_m A_n$ of satellites, where $m \neq n = \overline{1, N}$, N is the number of satellites, $C_N^2 = \binom{N}{2}$ InSAR baselines can be drawn.

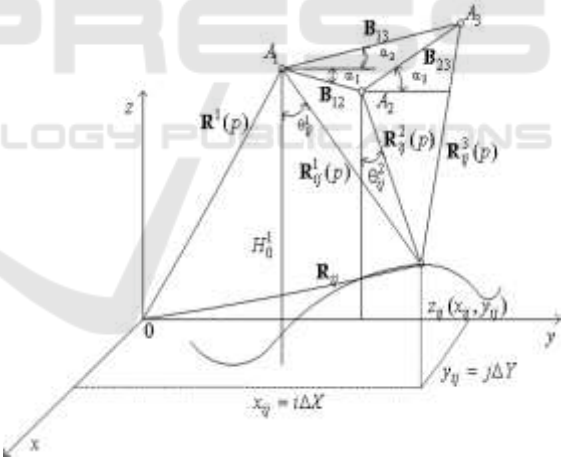

Figure 1: Geometry and kinematics of the interferometry SAR scenario.

The main geometrical characteristic of the SAR signal is the distance vector from the SAR system to each point scatterer of the scene of interest, defined as the vector difference

$$\mathbf{R}_{ij}^{n}(p) = \mathbf{R}^{n}(p) - \mathbf{R}_{ij} = \left[x_{ij}^{n}(p), y_{ij}^{n}(p), z_{ij}^{n}(p)\right]^{T} \quad (1)$$

where $n = 1 \div N$ is the number of SAR receiver $\mathbf{R}_{ij}$ is the distance vector of ij th point scatterer from the scene, and $\mathbf{R}^n(p)$ is the distance vector to the n-th SAR receiver, the point of observation in coordinate system $Oxyz$ (Fig. 1); $x_{ij}^n(p)$, $y_{ij}^n(p)$, $z_{ij}^n(p)$ are the current coordinates of the pixel from the scene in respect of the n-th SAR receiver, measured at p th moment of observation and defined as

$$\begin{aligned} x_{ij}^n(p) &= x^n(p) - x_{ij}, \\ y_{ij}^n(p) &= y^n(p) - y_{ij}, \\ z_{ij}^n(p) &= z^n(p) - z_{ij}, \end{aligned} \tag{2}$$

where $x_{ij} = i\Delta X$, $y_{ij} = j\Delta Y$, $z_{ij} = z_{ij}(x_{ij}, y_{ij})$ is the discrete coordinate defining a surface of the scene of interest, $x^n(p)$, $y^n(p)$, $z^n(p)$, are the instant coordinates of the n-th SAR receiver, defined be following equations

$$\begin{aligned} x^n(p) &= x_0^n - V_x p T_p, \\ y^n(p) &= y_0^n - V_y p T_p, \\ z^n(p) &= z_0^n - V_z p T_p, \end{aligned} \tag{3}$$

where x_0^n, y_0^n, z_0^n are the initial coordinates of the n-th SAR, measured at the initial moment, T_p is the time repetition period; p is the current number of the emitted pulse, $\mathbf{V} = [V_x, V_y, V_z]^T$ is the vector velocity of the InSAR multi satellite system, $V_x = V\cos\alpha$, $V_y = V\cos\beta$, $V_z = V\cos\delta$ are the components of vector velocity, $\cos\alpha$, $\cos\beta$, $\cos\delta = \sqrt{1 - \cos^2\alpha - \cos^2\beta}$ are the guiding cosines, and V is the module of the vector velocity, $\mathbf{V}$. Modulus of the current distance vector of the pixel in respect of the nth SAR's receiver antenna is defined by the equation

$$R_{ij}^n(p) = \left\{[x_{ij}^n(p)]^2 + [y_{ij}^n(p)]^2 + [z_{ij}^n(p)]^2\right\}^{\frac{1}{2}} \tag{4}$$

The expression (4) can be used to model a SAR signal return from the ij-th point scatterer to the n-th receiver by calculation of the respective time delay and phase of the signal.

2.2 InSAR Geometrical Relations

The relations between two the distances to ijth pixel from mth and nth SAR receivers can be defined from Fig. 1 by application of the cosines theorem, i.e.

$$R_{ij}^n = \left\{\begin{array}{l}\left(R_{ij}^m\right)^2 + B_{mn}^2 - \\ 2B_{mn}R_{ij}^m\cos\left[\dfrac{\pi}{2} - [\theta^m{}_{ij} - \alpha_{mn})]\right]\end{array}\right\}^{\frac{1}{2}}, \tag{5}$$

where B_{mn} is the modulus of baseline vector, $\theta^m{}_{ij}$ is the look angle, α_{mn} is a priory known tilt angle, the angle between baseline vector and plane xOy. From (5) can be extracted expressions for calculation of the look angle $\theta^m{}_{ij}$ and height $h^m{}_{ij}$ of a ij-th pint scatter on the surface with respect to m-th receiver

$$\theta^m{}_{ij} = \alpha_{mn} + \arcsin\frac{[R_{ij}^m]^2 + B_{mn}^2 - [R_{ij}^n]^2}{2B_{mn}R_{ij}^m}, \tag{6}$$

$$z_{ij} = H^m{}_0 - R_{ij}^m\cos\theta^m{}_{ij}. \tag{7}$$

The path length from the transmitter A_1 to ij-th pixel on the scene and back to the receiver A_n where ($n = 1 \div N$), is $R_{ij}^{1n} = R_{ij}^1 + R_{ij}^n$. The difference between two the distances R_{ij}^{1n} and R_{ij}^{1m} is equal to $R_{ij}^{1n} - R_{ij}^{1m} = R_{ij}^n - R_{ij}^m$.

Denote the path difference between R_{ij}^m and R_{ij}^n as ΔR_{ij}^{mn}, i.e.

$\Delta R_{ij}^{mn} = R_{ij}^n - R_{ij}^m$, then

$R_{ij}^n = R_{ij}^m + \Delta R_{ij}^{mn}$.

Substitute $R_{ij}^n = R_{ij}^m + \Delta R_{ij}^{mn}$ in (6) and (7), then

$$\theta^m{}_{ij} = \alpha + \arcsin\left[\frac{B_{mn}}{2R_{ij}^m} - \frac{\Delta R_{ij}^{mn}}{B_{mn}} - \frac{[\Delta R_{ij}^{mn}]^2}{2B_{mn}R_{ij}^m}\right] \tag{8}$$

$$z_{ij} = H^m{}_0 - R_{ij}^m \times$$

$$\times\cos\left\{\alpha_{mn} + \arcsin\left[\frac{B_{mn}}{2R_{ij}^1} - \frac{\Delta R_{ij}^{mn}}{B_{mn}} - \frac{[\Delta R_{ij}^{mn}]^2}{2B_{mn}R_{ij}^m}\right]\right\} \tag{9}$$

The path difference ΔR_{ij}^{mn} in equations (8) and (9) can be expressed by the corresponding phase difference $\Delta\varphi_{ij}^{mn} = \frac{2\pi}{\lambda}\Delta R_{ij}^{mn}$ as $\Delta R_{ij}^{mn} = \frac{\lambda}{2\pi}\Delta\varphi_{ij}^{mn}$. If the current distance R_{ij}^{m} can be measured expressions (8) and (9) can be written as follows

$$\theta^{m}{}_{ij} = \alpha_{mn} + \arcsin\left[\begin{array}{l}\frac{B_{mn}}{2R_{ij}^{m}} \\ -\frac{\lambda}{2\pi B_{mn}}\Delta\varphi_{ij}^{mn}\left(1+\frac{\lambda}{4\pi R_{ij}^{m}}\Delta\varphi_{ij}^{mn}\right)\end{array}\right] \quad (10)$$

$$z_{ij} = H^{m}{}_{0} - R_{ij}^{m} \times \cos\left\{\alpha_{mn} + \arcsin\left[\begin{array}{l}\frac{B_{mn}}{2R_{ij}^{m}} - \frac{\lambda}{2\pi B_{mn}}\Delta\varphi_{ij}^{mn}\times \\ \times\left(1+\frac{\lambda}{4\pi R_{ij}^{m}}\Delta\varphi_{ij}^{mn}\right)\end{array}\right]\right\} \quad (11)$$

Using expressions (10) and (11) the elevation look angle $\theta^{m}{}_{ij}$ and the height z_{ij} of the particular pixel can be calculated.

3 SAR TRANSMITTED LFM WAVEFORM AND DETERMINISTIC SIGNAL MODEL

The SAR transmits a series of electromagnetic waveforms to the surface, which are described analytically by the sequence of linear frequency modulation (LFM) (chirp) pulses as follows

$$S(t) = \sum_{p=1}^{M} A\exp\left\{-j\left[\omega(t-pT_p) + b(t-pT_p)^2\right]\right\}, \quad (12)$$

where A is the amplitude of the transmitted pulses, T_p is the pulse repetition period, $\omega = 2\pi\frac{c}{\lambda}$, is the signal angular frequency, $p = \overline{1, M}$ is the current number of emitted LFM pulse, M is a full number of emitted pulses during aperture synthesis, $c = 3.10^{8}$ m/s is the speed of the light, ΔF is the bandwidth of the transmitted pulse that provides the dimension of the range resolution cell, i.e. $\Delta R = c/2\Delta F$, $b = \frac{\pi\Delta F}{T}$ is the LFM rate, T is the time duration of a LFM pulse.

The deterministic component of SAR signal, reflected by ij-th pixel can be determined by expression

$$S_{ij}^{n}(t) = a_{ij}(z_{ij})\mathbf{rect}\frac{t-t_{ij}^{n}}{T}\times \exp\left\{-j\left[\begin{array}{l}\omega\left(t-t_{ij}^{n}\right) \\ +b(t-t_{ij}^{n})^2\end{array}\right]\right\} \quad (13)$$

where

$$\mathbf{rect}\frac{t-t_{ij}^{n}(p)}{T} = \begin{cases}0, \frac{t-t_{ij}^{n}(p)}{T} \le 0 \\ 1, \frac{t-t_{ij}^{n}(p)}{T} \le 1 \\ 0, \frac{t-t_{ij}^{n}(p)}{T} > 1\end{cases}, \quad (14)$$

where $a_{ij}(z_{ij})$ is the reflection coefficient of the pixel from the surface. The parameter $a_{ij}(z_{ij})$ is a function of surface geometry; $t_{ij}^{n}(p) = \frac{R_{ij}^{1}(p) + R_{ij}^{n}(p)}{c}$ is the signal time delay from the ij th point scatterer measured on the nth receiver.

The deterministic components of the SAR signal return are derived by applying the physical optic's principle of Huggens-Fresnel, according to which the SAR signal return can be calculated as a sum of elementary signals reflected by point scatterers from the surface, i.e. the time record of data $S^{n}(p,k)$ can be written as

$$S^{n}(t) = \sum_{i}\sum_{j} a_{ij}(z_{ij})\mathbf{rect}\frac{t-t_{ij}^{n}}{T}\exp\left\{-j\left[\begin{array}{l}\omega\left(t-t_{ij}^{n}\right) \\ +b(t-t_{ij}^{n})^2\end{array}\right]\right\} \quad (15)$$

The time dwell t of the SAR signal return for each transmitted pulse p can be expressed as $t = (k - k_{ij\min})\Delta T$, where $k = \overline{k_{ij\min}(p), k^n_{\max}(p)}$ is the sample number of the SAR return, $k_{ij\min} = \text{int}[t_{ij\min}(m)/\Delta T]$, $\Delta T = 1/2\Delta F$ is the sample time duration of the return, ΔF is frequency bandwidth, $k^n_{\max}(p)$ is the number of the last range bin where SAR return is registered in n-th receiver for each emitted pulse. Hence, SAR return registered in n-th receiver in discrete form can be written as

$$\dot{S}^n(p,k) = \sum_i \sum_j a_{ij}(z_{ij}) \mathbf{rect} \frac{t - t^n_{ij}}{T} \times \exp\left\{ -j \begin{bmatrix} \omega\left((k-1)\Delta T - t^n_{ij}(p)\right) \\ +b\left((k-1)\Delta T - t^n_{ij}(p)\right)^2 \end{bmatrix} \right\} \quad (16)$$

The expressions (1) - (16) can be used for modeling the SAR signal return in case the satellites are moving on rectilinear trajectory in 3-D coordinate system.

4 SAR IMAGE RECONSTRUCTION, COREGISTRATION AND SAR INTEREFEROGRAM GENERATTION

4.1 SAR Image Reconstruction Algorithm

Image reconstruction is constituted by following operations: frequency demodulation; range compression; coarse range alignment and precise phase correction, and azimuth compression. The result is a complex image of the scene.

In each SAR receiver a frequency demodulation is carried out. It is performed by multiplication of the right term of equation (10) with a complex conjugate exponential function

$$\exp\left\{ j\left(\omega(k-1)\Delta T + b[(k-1)\Delta T]^2\right)\right\}.$$

Thus, the range distributed frequency demodulated SAR return in n-th receiver for p-th pulse can be written as

$$\hat{\dot{S}}^n(p,k) = \sum_i \sum_j a_{ij}(z_{ij}) \mathbf{rect} \frac{(k-1)\Delta T - t^n_{ij}}{T} \times \exp\left\{ -j\left[\omega t^n_{ij}(p) + b\left((k-1)\Delta T - t^n_{ij}(p)\right)^2 \right] \right\} \quad (17)$$

SAR data refer to a set of data that has a real (Cosine, In-phase) and imaginary (Sine, Quadrature) component. Both this components of backscattered signals are measured by each SAR receiver. Therefore, the SAR data stream from each receiver can be writes as

$$\hat{\dot{S}}^n(p,k) = I^n(p,k) + jQ^n(p,k) \quad (18)$$

where

$I^n(p,k) = \text{Re}[\hat{\dot{S}}^n(p,k)]$ is the In-phase part of the SAR signal in the nth receiver,

$Q^n(p,k) = \text{Im}[\hat{\dot{S}}^n(p,k)]$ is the Quadrature part of the SAR signal in the nth receiver,

Range compression is implemented by cross correlation of the complex SAR signal and reference function, $\exp\left\{jb[(k-1)\Delta T]^2\right\}$ or by Fourier transform of LFM demodulated SAR signal, using the expressions as follows.

- cross correlation

$$\dot{S}^n_R(p,\hat{k}) = \sum_{k=1}^{K} \hat{\dot{S}}^n(p,k) \exp\left\{jb[(k-\hat{k}-1)\Delta T]^2\right\} \quad (19)$$

where K is the full number of LFM samples, range bins where SAR signal is registered;

- Fourier transform

$$\dot{S}^n_R(p,\hat{k}) = \sum_{k=1}^{K} \hat{\dot{S}}^n(p,k).\exp\left(j\frac{2\pi k\hat{k}}{K^n_{\max}} \right), \quad (20)$$

for each $p = \overline{1, M}$ and $\hat{k} = \overline{1, K}$.

Range alignment and phase correction is implemented by well known range alignment and focusing procedures [Lazarov, A. 2002].

Azimuth compression is implemented by Fourier transform of the range compressed signal, $\dot{S}^n_R(p,\hat{k})$. It yields a complex image based on the n-th receiver data and can be expressed as

$$\dot{I}^n(\hat{k},\hat{p}) = \sum_{p=1}^{M} \dot{S}^n_R(p,\hat{k}) \exp\left(j\frac{2\pi p\hat{p}}{M} \right), \quad (21)$$

for each $\hat{p} = \overline{1, M}$, $\hat{k} = \overline{1, K}$.

It is worth noting that the complex pixel of the SAR image in *n*-th receiver preserves the phase information defined by path length from the transmitter to the *ij*-th pixel and back to the *n*-th SAR receiver. Based on the pixels phase information and precise co-registration of two complex images a complex interferogram can be generated.

4.2 Co-registration of Two SAR Complex Images

To generate an interferogram between two complex images first a precision under pixel co-registration for any pair of two complex images has to carry out (Guizar-Sicairos, M., 2008).

Let $I^n(\hat{k}.\hat{p})$ and $I^m(\hat{k}.\hat{p})$ be two complex images obtained by the *n*th and *m*th receiver, respectively, and let $i^n(q,r)$ and $i^m(q,r)$ be two complex spectrums of the images defined by the expressions

$$i^m(q,r) = \sum_{\hat{p}=1,}^{M}\sum_{\hat{k}=1}^{K} I^m(\hat{k}.\hat{p}) \exp\left[-j\left(\frac{2\pi\hat{k}q}{K} + \frac{2\pi\hat{p}r}{M}\right)\right],$$

$$i^n(q,r) = \sum_{\hat{p}=1,}^{M}\sum_{\hat{k}=1}^{K} I^n(\hat{k}.\hat{p}) \exp\left[-j\left(\frac{2\pi\hat{k}q}{K} + \frac{2\pi\hat{p}r}{M}\right)\right].$$

In case the image $I^m(\hat{k}.\hat{p})$ is displaced in respect of the image $I^n(\hat{k}.\hat{p})$ on intervals $\Delta\hat{k}$ and $\Delta\hat{p}$ it can be written

- in the space domain

$$I^m(\hat{k}.\hat{p}) = I^n(\hat{k}+\Delta\hat{k}, \hat{p}+\Delta\hat{p})$$

- in the frequency domain

$$i^m(q,r) = i^n(q,r) \exp\left[j\left(\frac{2\pi\Delta\hat{k}.q}{K} + \frac{2\pi\Delta\hat{p}.q}{M}\right)\right].$$

The level of coincidence of the complex images can be calculated in space and/or frequency (spectral) domain by cross-correlation and inverse Fourier transform of the multiplication of the two complex spectrums as follows

- in the space domain

$$C(\Delta\hat{k}, \Delta\hat{p}) = \sum_{\hat{p}=1}^{M}\sum_{\hat{k}=1}^{K} I^n(\hat{k}.\hat{p}).I^m(\hat{k}+\Delta\hat{k}, \hat{p}+\Delta\hat{p}),$$

where $\Delta\hat{k}$ varies from 0 to the pixel's dimension with step 1/10(pixel's dimension on $\hat{k}$ axis), $\Delta\hat{p}$ varies from 0 to the pixel's dimension with step 1/10(pixel's dimension on $\hat{p}$ axis);

- in the frequency domain

$$C(\Delta\hat{k}, \Delta\hat{p}) = \sum_{r=1}^{M}\sum_{q=1}^{K} i^m(q,r) i^n(q,r) \times \exp\left[j\left(\frac{2\pi(\hat{k}+\Delta\hat{k})q}{K} + \frac{2\pi(\hat{p}+\Delta\hat{p})r}{M}\right)\right].$$

Maximum of the correlation function corresponds to a maximum coincidence, i.e. the complex images are best co-registered.

After SAR image reconstructions complex interferograms can be generated by pixel-wise multiplication of the two complex SAR images. For example, the complex interferogram between *m*-th and *n*-th SAR complex image can be calculated by the expression

$$\dot{I}^{mn}(\hat{k}, \hat{p}) = \dot{I}^n(\hat{k}, \hat{p}) \otimes [\dot{I}^m(\hat{k}, \hat{p})]*, \qquad (22)$$

where $\otimes$ denotes elementwise product; the sign "*" denotes complex conjugate.

4.3 Iterative Procedure for Pixel Height Determination

Step $k = 0$

1. Consider *ij*-th pixel with coordinates $x_{ij}, y_{ij}, z_{ij} = 0$ (the pixel is on the base plane *xOy*).
2. Compute the distance R_{ij}^m

$$R_{ij}^m(0) = \left[\begin{matrix}\left(x_0^m - x_{ij}\right)^2 + \left(y_0^m - y_{ij}\right)^2 \\ + \left(z_0^m - z_{ij}\right)^2\end{matrix}\right]^{\frac{1}{2}},$$

where x_0^m, y_0^m and z_0^m are coordinates of *m*-th SAR at the moment *p*=*N*/2 (moment of image extraction).

Step $k = k$

3. Compute the distance R_{ij}^n

$$R_{ij}^n(k) = \left[\begin{matrix}\left(x_0^n - x_{ij}\right)^2 + \left(y_0^n - y_{ij}\right)^2 \\ + \left(z_0^n - z_{ij}\right)^2\end{matrix}\right]^{\frac{1}{2}},$$

where x_0^n, y_0^n and z_0^n are coordinates of *n*-th SAR at the moment *p*=*N*/2 (moment of image extraction).

4. On *k*-th step compute the interferometric phase:

$$\Delta\varphi_{ij}^{mn}(k) = \frac{2\pi}{\lambda}\Delta R_{ij}^{mn},$$

where $\Delta R_{ij}^{mn} = R_{ij}^{m} - R_{ij}^{n}$.

5. If $\Delta\varphi_{ij}^{mn}(k) < \Delta\varphi_{ij}^{mn}$, then

Step $k = k + 1$.

6. On (k + 1)-th step consider a pixel with coordinates $x_{ij}, y_{ij}, z_{ij}(k+1) = z_{ij}(k) + \Delta z$.
7. Go to point 2 and 3.
8. If $\Delta\varphi_{ij}^{mn}(k) > \Delta\varphi_{ij}^{mn}$, then consider the pixel with coordinates

x_{ij}, y_{ij}, $z_{ij}(k+1) = z_{ij}(k) + (\Delta z / r)$,

where $r = 2,3,4\ldots$

9. Go to point 2 and 3.
10. If $\Delta\varphi_{ij}^{mn}(k) = \Delta\varphi_{ij}^{mn}$, then $z_{ij}(k) = h_{ij}$.

Stop.

The height's estimation procedure can be applied either for all pixels or only for one pixel from the surface of interest. In the latter case a scale coefficient can be defined in order to transform unwrapped phase surface to topographic map.

5 NUMERICAL EXPERIMENT

To verify the correctness of the signal model and image reconstruction and co-registration algorithms numerical experiment is carried out.

Assume multi satellite InSAR system comprising three satellites, one with transmitter and receiver, two – only with receivers, with initial space coordinates as follows:

$$x_0^1 = 0 \text{ m};\ y_0^1 = 10.10^3 \text{ m},\ z_0^1 = 100.10^3 \text{ m},$$
$$x_0^2 = 0 \text{ m},\ y_0^2 = 10{,}1.10^3 \text{ m},\ z_0^2 = 100.10^3 \text{ m},$$
$$x_0^3 = 0 \text{ m},\ y_0^3 = 10{,}2.10^3 \text{ m},\ z_0^3 = 100.10^3 \text{ m},$$

and coordinates of vector-velocity of the three satellites: $v_x = 0$ m/s; $v_y = -600$ m/s; $v_z = 0$ m/s.

Multi satellite SAR system observes a surface (Fig. 2) depicted by equation

$$z_{ij} = 3(1 - x_{ij})^2 \exp[-x_{ij}^2 - (y_{ij} + 1)^2] -$$
$$-10\left(\frac{x_{ij}}{5} - x_{ij}^3 - y_{ij}^5\right)\exp(-x_{ij}^2 - y_{ij}^2) -,$$
$$-\frac{1}{3}\exp[-(x_{ij} + 1)^2 - y_{ij}^2]$$

where $x_{ij} = i\Delta X$, $y_{ij} = j\Delta Y$, $i = \overline{1, I}$, $j = \overline{1, J}$, I = 128 pixels; J = 128 pixels; ΔX; ΔY - the spatial dimensions of the pixels.

Normalized amplitude of reflected signals from every pixel $a_{ij} = 0.001$. Dimensions of the pixel are $\Delta X = \Delta Y = 2$ m. Wavelength is 0.03 m. Carrier frequency is 3.10^9 Hz. Frequency bandwidth is $\Delta F = 250$ MHz. Pulse repetition period is $T_p = 25.10^{-3}$ s. LFM pulse duration is $T = 5.10^{-6}$ s. Sample time duration is $\Delta T = 1{,}95.10^{-8}$ s. LFM samples are K = 512. Emitted pulses are M = 512. Digital geometry description and SAR signal modeling are performed based on the theory in sections III and IV. Complex images through correlation range compression and FFT azimuth compression are retrieved. Based on a priory known kinematical parameters of satellites and coordinates of reference point from the surface autofocusing phase correction of the SAR signals registered in the both receivers can be implemented.

The real and imaginary part of the complex signal measured in the first receiver is depicted in Fig. 2.

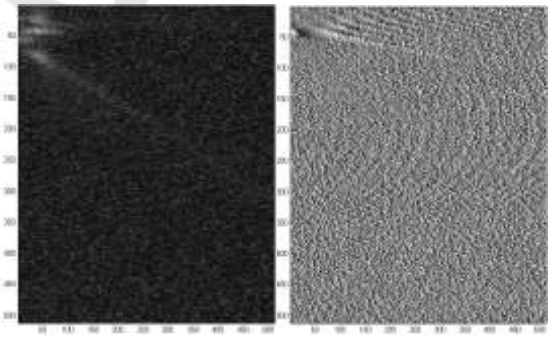

Figurre 2: Real and imaginary part of the complex signal measured in the first receiver.

The amplitude and phase of the reconstructed complex image obtained in the first receiver is depicted in Fig. 3. The position of the surface's image in the frame is defined by the position of the receiver satellite in the point of imaging of the

surface, as a rule, this point is in the middle of the synthetic aperture length.

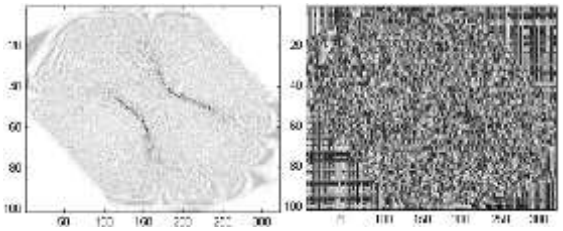

(*a*) (*b*)

Figure 3: The amplitude and phase of the reconstructed complex image obtained in the first receiver.

The real and imaginary part of the complex signal measured in the second receiver is depicted in Fig. 4.

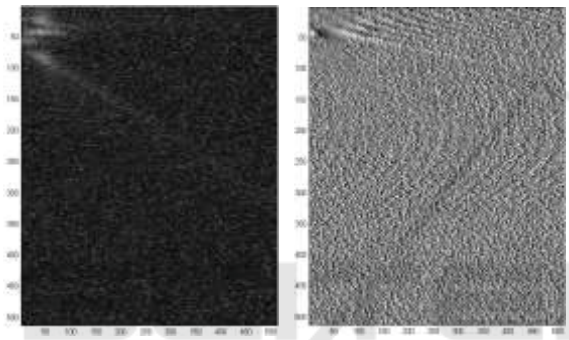

(*a*) (*b*)

Figure 4: Real (*a*) and imaginary (*b*) part of the complex signal measured in the second receiver.

The amplitude and phase of the reconstructed complex image obtained in the second receiver is depicted in Fig. 5. It can be noticed the shape of the surface is similar to the shape of the image obtained by the first receiver. In contrast, the phase pictures are different based on the different positions of both satellites in respect of the surface.

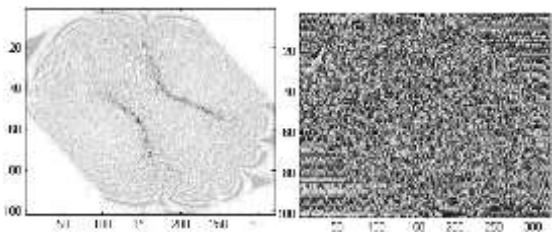

(*a*) (*b*)

Figure 5: The amplitude and phase of the reconstructed complex image obtained in the second receiver.

After co-registration of complex images obtained in the first and second receiver and complex interferogram generation the result as a coherent map (*a*) and interferometric phase (*b*) is depicted in Fig. 6.

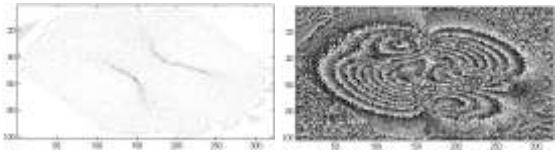

(*a*) (*b*)

Figure 6: Complex interferogram: coherent map and interferometric phase generated by the first and second complex images.

The real and imaginary part of the complex signal measured in the third receiver is depicted in Fig. 7.

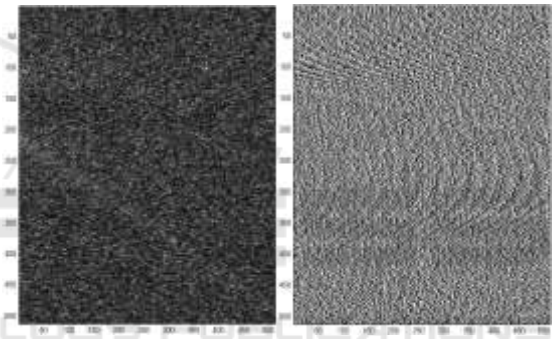

(*a*) (*b*)

Figure 7: Real and imaginary part of the complex signal measured in the third receiver.

The amplitude and phase of the reconstructed SAR complex image obtained in the third receiver is depicted in Fig. 8. It can be noticed the shape of the surface is similar to the shape of the image obtained by the first receiver. In contrast, the phase pictures are different based on the different positions of both satellites in respect of the surface.

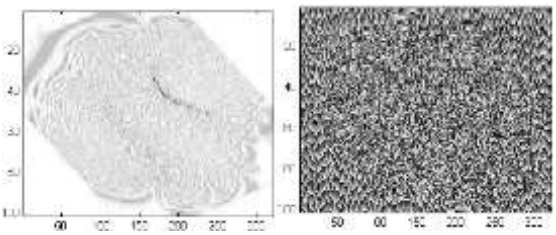

(*a*) (*b*)

Figure 8: The amplitude and phase of the reconstructed complex image obtained in the third receiver.

After co-registration of complex images calculated by the data obtained in the first and third receiver, and complex interferogram generation, the result as a coherent map (*a*) and interferometric phase (*b*) is depicted in Fig. 9.

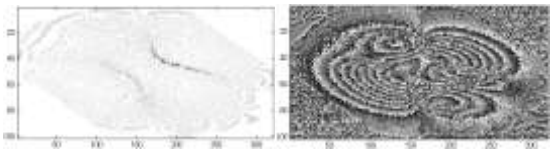

(*a*) (*b*)

Figure 9: Complex interferogram: coherent map and interferometric phase generated by the first and third complex images.

Comparing the interferometric phases presented in Fig. 6 and Fig. 9 it can be concluded that they are similar, i.e. very close to each other. It is a result of precise under pixel co-registrations of the first and second, and the first and third complex images.

6 CONCLUSIONS

In the paper a multi-satellite InSAR system has been analysed and numerically experimented. The geometry of InSAR scenario and kinematics of multiple SAR satellites has been analytically described. Mathematical expressions for current distances between SAR satellites and surface point scatterers are derived and principal InSAR parameters are defined. A model of linear frequency modulated SAR signal with InSAR applications, reflected from the topographic surface has been developed. Correlation and spectral SAR image reconstruction algorithms, co-registration, and iterative pixel height determination procedures have been described. Based on geometrical and kinematical models numerical interferograms of a topographic surface have been created.

REFERENCES

Rott, H., Nagler, T., Rocca, F., et al., 2003. InSAR techniques and applications for monitoring landslides and subsidence, in: Benes (Ed.), Geoinformation for European-wide integration, In Proceedings of *EARSeL Assembly, Prague*, June 2002. Millpress, Rotterdam, 25–31.

Massonet, D., Feigl, K.L., 1998. Radar interferometry and its application to changes in the Earth_s surface. *Rev. Geophys*., 36, 441–500, 1998.

Henry, E., Mayer, C., Rott, H., 2004. Mapping mining-induced subsidence from space in a hard rock mine: example of SAR interferometry application at Kiruna mine. *CIM Bull*. 97 (1083), 1–5.

Rott, H., Scheuchl, B., Siegel, A., et al., 1999. Monitoring very slow slope movements by means of SAR interferometry: a case study from a mass waste above a reservoir in the OË tztal Alps, Austria. *Geophys. Res. Let*. 26, 1629–1632.

Rott, H., Mayer, C., Siegel, A., 2000. On the operational potential of SAR interferometry for monitoring mass movements in Alpine areas, In Proceedings of *3rd European Conference on Synthetic Aperture Radar (EUSAR2000)*, Munich, May 2000, 43–46.

Berardino, P., M. Costantini, G. Franceschetti, A. Iodice, Pietrnera L. and Rizzo, V., 2002. Differential SAR interferometry for the study of slope instability at Maratea, Italy, in Proceedings of *International Geoscience and Remote Sensing Symposium*, Toronto, Canada, 2693-2695.

Berardino, P., M. Costantini, G. Franceschetti, A. Iodice, Pietrnera L. and Rizzo, V., 2003. Use of differential SAR interferometry in monitoring and modelling large slope instability at Maratea (Basilicata, Italy), *Eng. Geol.*, vol. 68, 2003, 31-51.

Graham, L.C., 1974. Synthetic Interferometer Radar for Topographic Mapping, *Proceedings of the IEEE*, vol.62, no.6, 1974. 763.

Zebker, H.A., Goldstein, R.M., 1986. Topographic Mapping from Interferometric Synthetic Aperture Radar Observations, *Journal of Geophys.Res*., vol.91, no. B5, 1986, 4993-4999.

Feigl, K.L., Sarti, F., Vadon, H. Durand, P., Mclusky S. et al., 2002. Estimating slip distribution for the Izmit mainshock from coseismic GPS, ERS-1, RADARSAT and SPOT measurements, *Bull. Seism. Soc. Amer*.

Gens, R., Van Genderen, J.L., 1996. Review article: SAR interferometry-issues, techniques, applications. *International Journal for Remote Sensing*, 17(10), 1803-1835.

Reilinger, R.E., Ergintav, S., Bürgmann, R., McClusky, S., Lenk, O., et al., 2000. Coseismic and postseismic fault slip for the 17 August 1999, M=7.4, Izmit, *Turkey earthquake, Science*, 289, 1519-1524.

Wright, T.J., Fielding, E.J., Parsons, B.E., and England, P.C., 1999. Triggered slip: observations of the 17 August 1999 Izmit (Turkey) earthquake using radar interferometry, *Geophys. Res. Lett.*, 28, , 2001, 1079-1082.

Weston, J., Ferreira, A.M.G., Funning, G. J., 2012. Systematic comparisons of earthquake source models determined using InSAR and seismic data, *Tectonophysics* 532–535, 61–81.

Feng, G., Hetland, E., Ding, X.L., Li, Z., Zhang, L., 2010. Coseismic fault slip of the 2008 Mw 7.9 Wenchuan earthquake estimated from InSAR and GPS measurements, *Geophysical Research Letters*, 37, L01302.

Liu-Zeng, J., Zhang, Z., Wen, L., Tapponnier, P., Sun, J., Xing, X., Hu, G., Xu, Q., Zeng, L., Ding, L., Ji, C., Hudnut, K.W., van der Woerd, J., 2009. Co-seismic rupture of the 12 May 2008, Ms 8.0 Wenchuan earthquake, Sichuan: east–west crustal shortening on oblique, parallel thrusts along the eastern edge of Tibet. *Earth and Planetary Science Letters* 286, 355–370.

Sudhaus, H., Jonsson, S., 2009. Improved source modelling through combined use of InSAR and GPS under consideration of correlated data errors: application to the June 2000 Kleifarvatn earthquake Iceland. *Geophysical Journal International* 176, 389–404.

Lazarov, A.D., Minchev, Ch., 2002. Correlation-autofocusing-spectral 2-D ISAR Image Reconstruction from Linear Frequency Modulated Signals, *21st Digital Avionics Systems Conference (DASC)*, Irvine, California, October 2002.

Guizar-Sicairos, M., Thurman, S.T., Fienup, J. R., 2008. Efficient subpixel image registration algorithms, *Opt. Lett.*, vol. 33, 156-158.